International Journal of Pharmaceutics xxx (xxxx) 122520

Contents lists available at ScienceDirect

International Journal of Pharmaceutics

journal homepage: www.elsevier.com/locate/ijpharm

Solid dispersions of atorvastatin with Kolliphor RH40: Enhanced supersaturation and improvement in a hyperlipidemic rat model

Carlos Torrado-Salmerón [a, c], Víctor Guarnizo-Herrero [a], Guillermo Torrado [b], M Ángeles Peña [b], Santiago Torrado-Santiago [a, c, *], Paloma Marina de la Torre-Iglesias [a, c]

[a] Department of Pharmaceutics and Food Technology, Faculty of Pharmacy, Complutense University of Madrid, Plaza Ramón y Cajal s/n, 28040 Madrid, Spain
[b] Department of Biomedical Science, Faculty of Pharmacy, University of Alcalá de Henares, Ctra Madrid-Barcelona Km 33,600, 28805 Madrid, Spain
[c] Instituto Universitario de Farmacia Industrial (IUFI), Complutense University of Madrid, Plaza Ramón y Cajal s/n, 28040 Madrid, Spain

ARTICLE INFO

Keywords:
Atorvastatin
Solid dispersion
Micellar system
Supersaturation
Hyperlipidemia
Liver steatosis

ABSTRACT

Atorvastatin is a potent lipid-lowering drug with poor solubility and high presystemic clearance that limits its therapeutic efficacy. The aim of this study was to develop solid dispersions and micellar systems to obtain fast-dissolving atorvastatin systems that enhances their anti-hyperlipidemic effect. Solubility and wettability studies allow the development of solid dispersions with low proportions of croscarmellose sodium as hydrophilic carrier. Solid state characterization studies indicated that the addition of Kolliphor® RH40 surfactant to solid dispersions increases intermolecular hydrogen bonding between drug and polymer chains. Dissolution studies in biorelevant Fasted State Simulate Intestinal Fluid (FaSSIF pH 6.5) medium showed for atorvastatin solid dispersion a supersaturation peak of atorvastatin followed by an aggregation/precipitation process. Only the presence of a surfactant such as Kolliphor® RH40 in atorvastatin micellar system, promotes the presence of micelles that achieve delayed recrystallization. Efficacy studies were carried out using a hyperlipidemic model of rats fed with a high- fat diet. The atorvastatin micellar system at doses of 10 mg/kg, revealed a significant improvement in serum levels of total cholesterol, low-density lipoproteins, and triglycerides compared to atorvastatin raw material. This micellar system also exhibited more beneficial effects on liver steatosis, inflammation and ballooning injury.

1. Introduction

Non-alcoholic fatty liver disease (NAFLD) encompasses the simple hepatic steatosis to more progressive steatosis with ballooning, and lobular inflammation with or without fibrosis (Doumas et al., 2018; Van den Hoek et al., 2021). Non-alcoholic steatohepatitis (NASH) was related to a hyperlipidemia characterized by a high level of cholesterol (TC), triglycerides (TG), and low-density lipoprotein (LDL) (Van den Hoek et al., 2021; Torrado-Salmerón et al., 2019).

Currently, treatment for NAFLD is generally dependent on gradual loss of body weight and change in lifestyle. However, these strategies have poor compliance in many patients (Torrado-Salmerón et al., 2019). Recently, several studies revealed that treatment with atorvastatin (AT) is effective and safe for patients with either NAFLD or NASH and hyperlipidemia (Doumas et al., 2018; Torrado-Salmerón et al., 2019).

AT is a potent inhibitor of HMG-CoA reductase, the limiting enzyme in cholesterol biosynthesis. AT is practically insoluble (< 0.1 mg/mL) in simulated gastric medium (Dong et al., 2018) and very slightly soluble in both distilled water (0.11–0.2 mg/mL) (Ha et al., 2014, Faraji et al., 2021; Srivalli and Mishra, 2015) and phosphate buffer pH 6.8 (0.29–0.32 mg/ml), respectively (Dong et al., 2018; Faraji et al., 2021). AT presents a low oral bioavailability (12 %), because of its low aqueous solubility, crystalline nature, hydrophobic character, rapid presystemic clearance in the gut wall and hepatic first-pass metabolism (Srivalli and Mishra, 2015; Elmowafy et al., 2017). Different strategies such as the development of nanocrystals and the elaboration of solid dispersions improve the solubility and dissolution rate of AT and proved to be adequate to increase its bioavailability. AT nanocrystallization techniques like milling or high-pressure homogenization allow to obtain important decrease in AT crystallinity (Tizaoui et al., 2020), and they have shown crucial increases on either solubility (Kurakula et

* Corresponding author at: Department of Pharmaceutics and Food Technology, Faculty of Pharmacy, Complutense University of Madrid, Plaza Ramón y Cajal s/n, 28040 Madrid, Spain.
E-mail addresses: ctorrado@ucm.es (C. Torrado-Salmerón), victor08@ucm.es (V. Guarnizo-Herrero), guillermo.torrado@uah.es (G. Torrado), angeles.pena@uah.es (M.Á. Peña), torrado2@ucm.es (S. Torrado-Santiago), pmtorre@ucm.es (P.M. de la Torre-Iglesias).

https://doi.org/10.1016/j.ijpharm.2022.122520
Received 6 July 2022; Received in revised form 25 November 2022; Accepted 16 December 2022
0378-5173/© 20XX

al., 2015), dissolution rate and also on enhancing its bioavailability (Sharma and Mehta, 2019; Kobayashi et al., 2017). The commercialized amorphous form of AT improves its solubility (0.36–0.54 mg/mL) (Kim et al., 2013; Jahangiri et al., 2015). However, this amorphous AT, formulated in nanoparticles, exhibits a high interparticle aggregation process which hinders its wettability and increases its recrystallization during dissolution studies (Kim et al., 2013; Rahman et al., 2020; Torrado-Salmerón et al., 2021). Hydrophilic polymers are currently used as carriers in solid dispersions due to their high hydrophilicity, water uptake capacity and plasticizing effect. Polymers such as polyvinylpyrrolidone (Kim et al., 2013; Jahangiri et al., 2015), hydroxypropyl methylcellulose (Kim et al., 2013) and polyethylene glycol (Faraji et al., 2021; da Silva et al., 2019) have been studied to produce AT solid dispersions.

In recent years, the use of different disintegrants such as sodium starch glycolate (Glycolys®) (SSG) (Agrawal et al., 2016), crospovidone (Polyplasdone® XL) (CP) (Chaturvedi et al., 2017; Indulkar et al., 2022) or sodium croscarmellose Solutab® (CCS) (Agrawal et al., 2016; Iqbal et al., 2020) have shown to be suitable as carriers in solid dispersions. The high-water uptake capacity of disintegrants can promote solubility of poorly soluble drugs. The interaction of disintegrants with surfactants rises the wettability surface (Chaturvedi et al., 2017; Indulkar et al., 2022) and improves the steric and electrostatic stabilization of the drug molecules within the amorphous structure of the polymer (Ma et al., 2018).

Although the nanoparticles lead to increased surface area, exposing more surfaces, which increases saturation coefficient and improves dissolution rate, these processes can also lead to a substantial rise in free Gibbs energy, making the formulation unstable. Surfactants act as stabilizers of solid dispersions by producing enough steric or electrostatic repulsion between particles to overcome agglomeration among them (Kurakula et al., 2015; Kobayashi et al., 2017). Ternary solid dispersions with low proportions of surfactants are showed in Table 1, which are characterized by lowering their surface tension, and improving their hydrophilicity and water uptake (Rahman et al., 2020). Different micellar solid dispersions have been studied using different excipients like sodium dodecyl sulphate (SDS) (da Silva et al., 2019; Agrawal et al., 2016), Poloxamer 188 (Dong et al., 2018; Sharma and Mehta, 2019), Pluronic® 127 or 68 (Shaker et al., 2020), polymers with high HLB values such as: Soluplus® (Ha et al., 2014; Rahman et al., 2020), Polyvinylpyrrolidone-vinyl acetate (PVP VA64) (Kim et al., 2013) and Gelucire® 48/16 (Aldosari et al., 2021). However, the high plasmatic clearance of AT and the complex hepatic mechanisms involved in the treatment of hyperlipidemia (Mohamed et al., 2019) have increased the tendency to evaluate the different systems developed through *in vivo* efficacy models (Sharma et al., 2019; Jarangiri et al., 2015; Kumar et al., 2017).

For studying micellar solid dispersions, is necessary to develop a dissolution method which will be able to simulate the gastrointestinal tract. The supersaturation conditions for AT solid dispersions in pH 6.8 phosphate buffer (Kim et al., 2013), water (Ha et al., 2014) and 0.1 N HCl (Shaker et al., 2020) displayed changes in AT release rate profiles. They were adequate for *in vitro* evaluating differences among several AT solid dispersions. Biorelevant dissolution medium has been used in dissolution studies for simulating fasted state in intestinal conditions (FaSSIF pH 6.5). This medium contains bile salts and phospholipids (Ikeuchi et al., 2018). The bile salts also have the capability to form mixed micelles in the gastrointestinal milieu. The use of FaSSIF pH 6.5 medium has shown to be adequate for observing crucial differences in ternary solid dispersions of low solubility drugs (Lakshman et al., 2020; Pas et al., 2020).

The disease severity of NASH was evaluated by NAFLD Activity Score (NAS). The use of NAS can be effective in evaluating the efficacy in the liver of different hydrophilic systems (Doumas et al., 2018; Torrado-Salmerón et al., 2019). Different studies indicate that the use of low proportions of surfactants in statins formulations produces an inhibitory effect on P-glycoproteins and modifies the CYP3A4 enzymes pathway which produces significant improvements in NASH disorders (Srivalli and Mirhra, 2015; Salama et al., 2018). The high values of alanine aminotransferase (ALT) and aspartate aminotransferase (AST) were related to oxidative stress and are related to the liver damage observed in the NAS score (Mohamed et al., 2019; Klaebel et al., 2019; Yin et al., 2019). The addition of low doses of surfactants to AT solid dispersions could be determinant for improvements in the NASH levels and may be particularly important in reducing the AT dose and decreasing its adverse effects (Salama et al., 2018).

The aim of this study was to develop AT solid dispersions with different hydrophilic superdisintegrants for selecting the most adequate on improving AT solubility in biorelevant FaSSIF pH 6.5 medium. The improvement on either the solubility and the supersaturation concentration during the dissolution rate, and the delay in the aggregation process in this biorelevant medium, were all investigated for micellar solid dispersions with polyoxyl 40 hydrogenate castor oil Kolliphor® RH40 (K) surfactant at different ratios. Different characterization stud-

Table 1
Composition of micellar solid dispersions formulations with low drug:surfactant ratios and their preparation methods, solubility results and dissolution conditions.

Preparation Methods	AT: Polymer: Surfactant	Solubility (mg/mL) (AT solubility increase)	Dissolution Test	Ref.
Spray-drying	AT:HPMC: SDS (1:1:0.1)	Water 1.4 (17.44-fold)	Water AT 20 mg/ 900 mL	Kwon et al., (2018)
Melting process	AT:PEG 10000: P 188 (1:5:1)	Water 0.273 ± 0.026 (1.36-fold) PBS (pH 6.8) 0.674 ± 0.067 (1.75-fold)	Water AT 20 mg/ 900 mL	Faraji et al., (2021)
Lyophilization technique	AT:SDS (1: 1)	---	Water AT 20 mg/ 900 mL	Da Silva et al., (2019)
Melting process	AT:Pluronic F127 (1:1) AT:Pluronic F68 (1:1)	Water 10 % F127 14.52 ± 0.84 (704-fold) Water 10 % F68 11.85 ± 0.63 (575-fold)	Supersaturation 0.1 N HCl AT40 mg/900 mL	Shaker et al., (2020)
Spray-drying	AT:Soluplus (1:1) to (1: 4)	Water 1 % ≈ 0.60 * (4-fold)	Supersaturation Water AT 300 mg/ 300 mL	Ha et al., (2014)
Solvent evaporation method	AT: Poloxamer 188 (1:1) to (1: 5)	Phosphate buffer pH 6.8 ≈ 0.61 (1.9-fold)	Phosphate buffer pH 6.8 AT 10 mg/ 900 mL	Dong et al., (2018)
Ball milling	---	Water AT 0.448 (3.7-fold)	Supersaturation Water AT 120 mg/ mL	Kobayashi et al., (2017)
SD / SAP *	AT:PVP VA64 (1:1) to (1: 5)	Water (1.4-fold)	Supersaturation Water AT 10 mg/ 900 mL	Kim et al., (2013)
Melting process	AT:Gelucire 48/16 (1:1) to (1: 7)	phosphate buffer pH 6.8 (1.95–9.3-fold)	Supersaturation Phosphate buffer pH 6.8 900 mL	Aldosari et al., (2021)
HPH / L **	AT: Poloxamer 188 (1:2) to (1: 5)	Phosphate buffer pH 6.8 (19.11-fold)	Dialysis bags Phosphate buffer pH 6.8 AT 50 mg/ 900 HCl	Sharma et al., (2019)

*SD / SAP. (Solid Dispersions / Supercritical antisolvent process).
**HPH / L. High pressure homogenization technique / Lyophilization process.

ies (FTIR, XRPD and DSC) have been carried out to relate, the physicochemical properties of both SD and MSD formulations, with the changes observed on their dissolution profiles. Finally, an hyperlipidemic rat model was selected to evaluate the improvement in lipid parameters efficacy and the decrease in hepatic steatosis for the selected micellar solid dispersion (MSD).

2. Materials and methods

2.1. Material

Atorvastatin (AT) was kindly supplied by Normon S.A. (Madrid, Spain). Excipients: sodium starch glycolate, Explotab® (SSG) was obtained from JRS Pharma (Patterson NY, USA); Sodium Croscarmellose, Ac-Di-Sol® SD-711 (CCS) was purchased from FMC Corporation (Philadelphia, PA, USA); Low-Hydroxypropyl Cellulose LH-21 (L-HPC) was kindly provided by Shin-Etsu Chemical Co., ltd. (Tokyo, Japan); Crospovidone, Polyplasdone® XL (CP) was provided by Ashland (DA, USA); Sodium dodecyl sulfate (SDS); Sodium taurocholate (NaTC) and Lecithin (LCT) were obtained from Sigma-Aldrich® (Madrid, Spain); Egg lecithin–Lipoid EPCS, Lipoid® (GmbH, Germany), Polyoxyl 40 hydrogenate castor oil (Kolliphor® RH40) BASF Chemical Company (Barcelona Spain) and Acetonitrile, Sodium hydroxide, Potassium phosphate monobasic, were obtained from Panreac® (Barcelona, Spain). Water was ultra-pure (Milli-Q) laboratory grade.

2.2. Methods

2.2.1. Preparation of formulations

AT raw material (AT-RM) was used as reference in either the characterization, dissolution, biochemical and efficacy studies.

Physical mixtures of AT: PM-AT:CCS:K (1:1:0.1) and PM-AT:CCS:K (1:1:0.3) were prepared as follows: 100 mg of AT and 100 mg of croscarmellose sodium were mixed with 10 mg or 30 mg of Kolliphor® RH40 in a ceramic bowl using a polymeric spatula.

The solid dispersion of atorvastatin (SD-AT) was made following a similar process. A solution of 100 mg of AT in 500 mL of ethanol was mixed in a ceramic bowl using a polymeric spatula with 100 mg of different disintegrants, such as: sodium croscarmellose for SD-AT:CCS (1:1); sodium starch glycolate for SD-AT:SSG (1:1); crospovidone for SD-AT:CP (1:1) and Low-Hydroxypropyl Cellulose LH-21 for SD-AT:L-HPC (1:1). Solid dispersion was dried at 40 °C for 24 h. The final product was screened to isolate the 0.297–0.840 mm fraction by sieving.

Ternary solid dispersions (micellar solid dispersions, MSD) were prepared containing AT:CCS:Kolliphor® RH40 with two ratios: MSD-AT:CCS:K (1:1:0.1) and MSD-AT:CCS:K (1:1:0.3) (w/w). The procedure was as follows: 100 mg of AT were added to 500 mL of ethanol solution with different proportions of surfactants and dissolved by vortexing (Fisherbrand™; Milan, Italy) at 2500 rpm for 2 min. The AT solution was mixed (in a ceramic bowl using a polymeric spatula) with 100 mg of croscarmellose as a hydrophilic carrier, dried at 40 °C for 24 h, and then sieved (0.840 mm). The final product was screened to isolate the 0.297–0.840 mm fraction by sieving.

2.2.2. Solubility, wettability and wetting time studies

Solubility studies were performed using excess amounts of each formulation, which were added to test tubes containing 3 mL of either FaSSIF pH 6.5 medium or pH 6.5 phosphate buffer. The tubes were mixed in a vortex and placed in a shaking water bath at 37 °C for five days, then the samples were filtered through a 0.45 μm filter (Acrodisc®, Port Washington, NY, USA). Each determination was performed in triplicate, and the error bars on the graphs represent the standard deviation. The sample quantification was carried out by HPLC (Agilent® 1100 series FLD G1321A) equipped with a 50 μL loop. Samples were separated using a Zorbax SB C-8 column (4.6 × 250 mm, 5 μm). The mobile phase consisted of pH 4.0 acetate buffer (40 %) and HPLC-grade acetonitrile (60 %), with a flow rate of 1 mL/min. Atorvastatin was analyzed with a UV–VIS detector at a wavelength of 241 nm. The analytical method was validated according to ICH Q2 (R1) (CPMP/ICH/381/95).

Wettability studies: a portion of tissue paper folded twice was placed in a Petri dish of 6 mm diameter and containing 3 mL of FaSSIF pH 6.5 medium, where the following samples were evaluated: AT raw material (AT-RM), pure croscarmellose sodium (CCS), physical mixture PM-AT:CCS:K (1:1:0.3), solid dispersions SD-AT:CCS (1:1), SD-AT:SSG (1:1), SD-AT:CP (1:1) and SD-AT:L-HPC (1:1) and the solid micellar dispersions MSD-AT:CCS:K (1:1:0.1) and MSD-AT:CCS:K (1:1:0.3) were evaluated. The medium absorption ratio, R, was determined using the equation (1):

$$R = (W_b - W_a)/W_a x100 \quad (1)$$

Where W_a and W_b are the weight of the sample before medium absorption and after medium absorption, respectively.

*Wetting time (*min*):* The time required for complete wetting was determined. 100 mg of each formulation were weighed and deposited on a piece of tissue paper placed in a Petri dish of 6 mm diameter and containing 3 mL of FaSSIF pH 6.5 medium (Blasco et al., 2020).

For solubility, wettability and wetting time studies. Each determination at each time point was performed in triplicate and the error bars in the graphs represent the standard deviation.

2.2.3. Solid state characterization

2.2.3.1. FTIR study. Fourier transform infrared (FTIR) spectroscopy of AT raw material (AT-RM), pure sodium croscarmellose (CCS), the physical mixture of AT with CCS and Kolliphor® RH40; PM-AT:CCS:K (1:1:0.3), the solid dispersion SD-AT:CCS (1:1) and micellar solid dispersions MSD-AT:CCS:K (1:1:0.3) were performed with FTIR-8400 S (Shimadzu®; Kioto, Japan). Samples were mixed with KBr powder (2:100) and compressed into 10 mm discs. The scanning range was 400–4000 cm^{-1} with a spectral resolution of 4 cm^{-1}.

2.2.3.2. X-ray powder diffraction (XRPD). The XRPD patterns were recorded on a Philips X'Pert-MPD X-ray diffractometer (Malvern Panalytical, Almelo, the Netherlands), in the CAI XRD (UCM, Madrid, Spain). The samples were irradiated with monochromatized CuKα radiation (λ = 1.542 Å) and analyzed between the 5 and 35° (2θ) degree range, scanning at a step size of 0.04° and a time of 1 s per step in all cases. The voltage and current used were 30 kV and 30 mA, respectively.

2.2.3.3. Differential scanning calorimetry (DSC). Samples were mounted on a TC 15 thermal analyzer (Mettler Toledo, Schwerzenbach, Switzerland). The temperature was calibrated using the indium reference standard. Samples were accurately weighed into aluminum pans, then hermetically sealed with aluminum lids, and heated from 25 °C to 250 °C at a heating rate of 10 °C/min under constant purging of dry nitrogen at 20 mL/min. An empty pan sealed in the same way as the samples was used as a reference.

2.2.4. Dissolution studies

AT raw material and the different formulations were evaluated in a biorelevant media under non-sink conditions. The dissolution study of the different formulations was performed at 100 rpm and 37.0 ± 0.5 °C using a magnetic stirrer thermostatic bath (FisherbrandTM; Milan, Italy). Amounts equivalent to 200 mg of AT were added in 200 mL of FaSSIF pH 6.5 (fasted state simulated intestinal fluid). This amount of atorvastatin and the volume of dissolution medium were selected for an adequate study of supersaturation and precipitation (França et al., 2018). Biorelevant media were prepared following the previously described methods (Torrado-Salmerón et al.,

2021; Lakshman et al., 2020). At different times, 0.5 mL samples were withdrawn and filtered through 0.45 μm (Acrodisc®, NY, USA), and 0.3 mL was discarded before collecting the final 0.2 mL of filtrate. The filtered samples were immediately diluted and analyzed by the HPLC method described in the solubility study. Each determination at each time was performed in triplicate, and the error bars on the graphs represent the standard deviation.

2.2.5. Animal studies

2.2.5.1. Experimental protocol. Twenty-four male Wistar rats weighing between 200 and 250 g were supplied from Envigo Rms Co., ltd. (Barcelona, Spain). The study was carried out in the Animal Experimentation Centre at the University of Alcalá de Henares following the Ethical Committee Regulations of the University, Community of Madrid PROEX 041/18, project identification code ES-280050001165 (27 April 2018). The animals were housed in standard cages in 12 h light–dark cycles and had unrestricted access to food and water throughout the experiment. The animals in the study were fed on a high-fat diet (HFD) composed of fats and cholesterol (18 g of fat, 2 g of cholesterol and 0.2 g of colic acid per 100 g of diet) for eight weeks. Experiments were performed on four groups of animals (n = 6). At the end of the eight weeks of feeding with a HFD, the serum lipid profile was measured for the induction of hyperlipidemia. Treatments of AT-RM and MSD-AT:CCS:K (1:1:0.3) formulation, equivalent to a 10 mg/kg dose of AT, were suspended in a sodium carboxymethylcellulose solution (0.75 % w/v) and 0.4 mL of the treatments were administered to the rats through oral gavage. The hyperlipidemic control group received only 0.4 mL of the sodium carboxymethylcellulose solution (0.75 % w/v). After four weeks of treatment, the animals were anesthetized and sacrificed by cardiac puncture to collect the blood of each animal.

2.2.5.2. Lipid profile analysis. Blood samples were taken after fasting for 15 h, and the serum was obtained by centrifugation at 2500 rpm for 10 min. Concentrations of total cholesterol (TC), triglycerides (TG), high-density lipoprotein (HDL), aspartate transaminase (AST), and alanine transaminase (ALT) were measured using commercial diagnostic kits, and the data were represented as mean mg/dL ± standard deviation. Low-density lipoprotein (LDL) concentrations were calculated using the Friedewald equation.

2.2.5.3. Histological analysis. A 5 mm thick section of liver tissue was cut and fixed in 40 g/L buffered formaldehyde and embedded in paraffin. The sections were stained with hematoxylin and eosin using a morphological semi-quantitative approach and graded as follows: steatosis: 0–3; inflammation: 0–3; ballooning: 0–2 (Yin et al., 2019). The histological evaluation of the liver sections was performed by an experimental pathologist. A threshold value of ≥ 5 indicated to correlate with the diagnosis of NASH.

2.2.5.4. Statistical analysis. In the *in vitro* studies, differences between obtained values (Mean ± SE) for the prepared formulae and the control formulae were carried out using one-way analysis of variance (ANOVA). Lipid Profile and histological analysis were evaluated by Tukey's test, with a one-way ANOVA test using Statgraphics (Statgraphics Technologies, The Plains, VA, USA).

3. Results

3.1. Drug solubility and wettability studies

In Table 2 it is shown the water uptake, wetting time and apparent solubility of either AT raw material (AT-RM), physical mixture: PM-AT:CCS (1:1), solid dispersions: SD-AT:CCS (1:1), SD-AT:SSG (1:1), SD-AT:CP (1:1) and SD-AT:L-HPC (1:1) and micellar solid dispersions for ratios: MSD-AT:CCS:K (1:1:0.1) and MSD-AT:CCS:K (1:1:0.3).

Table 2
Solubility (mg/mL) in phosphate buffer pH 6.5 and FaSSIF pH 6.5, Water uptake (%) and Wetting time (min) in FaSSIF pH 6.5 for AT raw material and the different formulations.

Formulations	Solubility phosphate buffer pH 6.5 (mg/mL)	Solubility FaSSIF pH 6.5 (mg/mL)	Water uptake FaSSIF pH 6.5 (%)	Wetting time FaSSIF pH 6.5 (min)
AT-RM	0.362 ± 0.010	0.416 ± 0.014	----	> 15
CCS	----	----	584.33 ± 43.56	1.35
PM-AT:CCS:K (1:1:0.3)	0.371 ± 0.017	0.418 ± 0.017	----	> 15
SD-AT:CCS (1:1)	0.423 ± 0.010	0.510 ± 0.004	468.00 ± 12.00	2.66
SD-AT:SSG (1:1)	0.412 ± 0.020	0.465 ± 0.010	420.67 ± 10.89	2.12
SD-AT:CP (1:1)	0.404 ± 0.026	0.461 ± 0.014	----	> 15
SD-AT:L-HPC (1:1)	0.437 ± 0.004	0.459 ± 0.009	----	> 15
MSD-AT:CCS:K (1:1:0.1)	0.379 ± 0.007	0.414 ± 0.016	660.00 ± 6.00	1.70
MSD-AT:CCS:K (1:1:0.3)	0.436 ± 0.006	0.441 ± 0.009	639.67 ± 14.22	0.92

AT-RM is a weak acid drug with a solubility of 0.362 ± 0.010 mg/mL in a pH 6.5 medium. A high increase in its partial solubility of 0.415 ± 0.014 mg/mL was observed in biorelevant FaSSIF pH 6.5 medium compared to phosphate buffer at pH 6.5. The hydrophobic behavior of AT-RM was confirmed by the absence of changes during the swelling process and showed high wetting times (>15 min), while the hydrophilic carrier CCS in FaSSIF pH 6.5 exhibits higher medium absorption and faster wetting time (1.35 min). The solubility values of AT-RM in both pH 6.5 phosphate buffer and FaSSIF pH 6.5 medium, observed in Table 2, were higher than those observed by different authors for crystalline AT calcium trihydrate in distilled water or in neutral pH medium (Kobayashi et al., 2017; Torrado-Salmerón et al., 2021). The use of an AT amorphous form, confirmed by DSC and RX studies, improves wettability and increments its solubility values (Kim et al., 2013; Torrado-Salmerón et al., 2021). Furthermore, the enhanced solubility of AT-RM in FaSSIF pH 6.5 medium compared to pH 6.5 phosphate buffer has been previously observed with several lipophilic drugs (Pas et al., 2020; Krollik et al., 2022). The presence of bile salts and lecithin micelles within the FaSSIF pH 6.5 increase the solubility of lipophilic drugs as AT by micellar solubilization (Aldosari et al., 2021; Lakshman et al., 2020).

PM-AT:CCS:K (1:1:0.3) physical mixture showed slow wetting times (>15 min) and only slightly improved AT solubility values (Table 2). The presence of hydrophilic carriers in physical mixtures provide a partial improvement on AT solubility (da Silva et al., 2019; Iqbal et al., 2020; Kwon et al., 2019).

The degree of AT solubility for the solid dispersions showed a significant increase ($p < 0.05$) compared to AT-RM (see Table 2). The slight increases observed between the solid dispersions in phosphate buffer pH 6.5, presented the following order: SD-AT:CP (1:1) < SD-AT:SSG (1:1) < SD-AT:CCS (1:1) < SD-AT:L-HPC (1:1) at pH 6.5. However, in biorelevant FaSSIF medium, a significant increase in partial solubility was observed (Table 2), presenting slight changes in the following order: SD-AT:L-HPC (1:1) < SD-AT:SSG (1:1) < SD-AT:CCS (1:1) ≤ SD-AT:CP (1:1). Solid dispersions showed a significant increase ($p < 0.05$) in solubility values in FaSSIF medium pH 6.5 compared to phosphate buffer pH 6.5. The presence of bile salts and lecithin micelles within FaSSIF pH 6.5 increase the solubility of lipophilic drugs in biorelevant media such as FaSSIF pH 6.5 (Lakshman et al., 2020; Krollik et al., 2022). The great increase in AT solubility values for solid dispersions

with hydrophilic carries CCS and SSG showed high medium uptake values of 468.00 ± 12.00 and 420.67 ± 10.89 for SD-AT:CCS (1:1) and SD-AT:SSG (1:1) respectively, which are related to important decreases in wetting times. These changes indicate that the dynamic immersion process of hydrophilic ionic chains of CCS and SSG plays a central role to increase the ability on the surface of AT powder to enter the FaSSIF solution from the air–water interface. However, a relevant decrease in the medium uptake values for SD-AT:CP (1:1) and SD-AT:L-HPC (1:1), was attributed to the higher viscosity of these systems, which was confirmed by high delays in the wetting time results (>15 min). In FaSSIF pH 6.5 medium, the high separation of hydrophilic chains accelerates the wetting times, improving the micellar solubilization effect by bile salts and providing an inhibition of hydrophobic drugs precipitation (Yin et al., 2019; Zarmpi et al., 2020).

The presence of low proportions of surfactant in the micellar solid dispersions MSD-AT:CCS:K (1:1:0.1) and MSD-AT:CCS:K (1:1:0.3) showed a clear change for AT apparent solubility (see Table 2). The MSD-AT:CCS:K (1:1:0.1) formulation showed a decrease in AT solubility compared to SD-AT:CCS (1:1) at both media (phosphate buffer of pH 6.5 and FaSSIF pH 6.5 respectively), indicating a negative effect of Kolliphor® RH40 surfactant on AT solubility for MSD-AT:CCS:K (1:1:0.1). Moreover, MSD-AT:CCS:K (1:1:0.3) in phosphate buffer at pH 6.5, produced a slight increase in AT solubility compared to SD-AT:CCS: (1:1). Whereas, in FaSSIF pH 6.5 medium, this micellar system exhibited a significant ($p < 0.05$) decrease in solubility values compared to SD-AT:CCS (1:1). System with high surfactant ratio, MSD-AT:CCS:K (1:1:0.3), showed a slighter increment for AT solubility compared to SD-AT:CCS: (1:1) in phosphate buffer at pH 6.5. In these systems, the surfactant favors the presence of hydrophilic chains particles on the surface of AT particles (Kwon et al., 2019; Sarabu et al., 2022). Meanwhile, in FaSSIF pH 6.5 biorelevant medium (see Table 2) after 5 days, the slight decrease in solubility observed was attributed to a depletion of supersaturation, which was related to a partial recrystallization of the drug in MSD-AT:CCS.:K (1: 1:0.3) (Lakshman et al., 2020). Previous studies have indicated that the presence of surfactants in the formulations produces high supersaturation values in dissolution studies but also produces slight decreases in solubility in different poorly soluble drugs such as ritonavir or posaconazole (Pas et al., 2020).

3.2. Characterization at the solid state

In FTIR spectrum data (Fig. 1), AT-RM exhibited the following peaks: broad absorption bands at 3403.57, 3241.51 and 3060.06 cm^{-1}, all of them due to N—H bending and asymmetric and symmetric O—H stretching; at 2962.44 cm^{-1} due to CH–stretching; two bands at 1667.71 and 1563.96 cm^{-1}, both of them due to asymmetric and symmetric C═O stretching of carbonyl group; 1436.73 cm^{-1} and 1313.01 cm^{-1} both due to O—H bending and C—O stretching of carboxylic acid; at 1224.05 and 1051.6 cm^{-1} both of them due to aromatic C—N and O—H stretching. These broad and strong absorption bands for the N—H and C═O groups could act as hydrogen bond acceptor and donor, respectively (Kumar et al., 2017; Li et al., 2021).

The FTIR spectrum of CCS (Fig. 1) showed absorption bands: at 3273.07 cm^{-1} due to symmetric O—H stretching; at 2927.61 cm^{-1} due to CH-stretching; two bands at 1619.98 and 1329.19 cm^{-1} both due to asymmetric and symmetric C═O stretching of carboxylic acid group and at 1058.37 cm^{-1} involving the C—O ether bond stretching (Li et al., 2021).

In comparison with the AT spectrum, PM-AT:CCS:K 1:1:0.3 formulation (Fig. 1), exhibited an intensity decrease on the resulting AT broad absorption bands: at 3410.90 cm^{-1} due to N—H bending; both at 3221.89 and 3060.44 cm^{-1} which were attributed to asymmetric and symmetric O—H stretching and at 2930.48 cm^{-1} attributed to symmetric C—H stretching characteristics. Moreover, no remarkable difference in peak positions for AT confirmed the compatibility of drug with

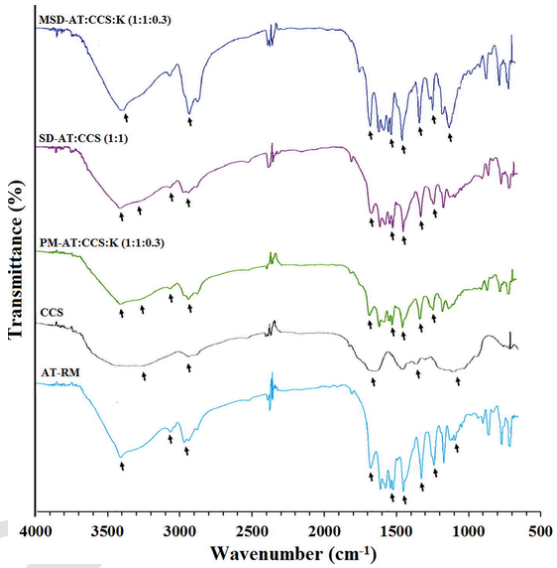

Fig. 1. FTIR spectra of Atorvastatin raw material (AT-RM); Croscarmellose (CCS); Physical mixture PM-AT:CCS:K (1:1:0.3); SD-AT:CCS (1:1); MSD-AT:CCS:K (1:1:0.1) and MSD-AT:CCS:K (1:1:0.3).

excipients in the formulation, showing the following peaks: at 1664.13 and at 1563.96 cm^{-1} due to asymmetric and symmetric C═O stretching region of carbonyl group; both at 1436.51 and 1313.15 cm^{-1} due to O—H and C—O stretching of carboxylic acid and at 1223.87 cm^{-1} due to aromatic C—N stretching. The decline observed in the intensity values for AT and CCS respective peaks were due to the dilution effect of CCS carrier in the formulation. The absence of interactions shown in the TFIR studies among hydrophilic CCS chains and AT molecules confirmed the compatibility of drug with excipients in formulation, (Li et al., 2021; Lakshman et al., 2020). Moreover, PM-AT:CCS:K 1:1:0.3 exhibited changes for the peaks at 3410.90 cm^{-1} and 2930.48 cm^{-1}, both of them assigned to N—H and the aliphatic chains, respectively, which were attributed to the presence of Kolliphor® RH40. These increases on FTIR peaks intensity corresponding to aliphatic chains, were also observed in formulations with different surfactants such as sodium dodecyl sulfate and sodium dodecyl sulphonate (Xu et al., 2019; Yang et al., 2019). In addition, in this diffractogram (Fig. 1), the reduction in magnitude of peaks due to the dilution effect of the hydrophilic carrier was observed (Li et al., 2021; Han et al., 2020).

SD-AT:CCS (1:1) solid dispersion showed a slight displacement, compared to AT-RM, for the following bands: at 3406.54, 3223.08 and 3061.18 cm^{-1}, which were assigned to N—H and asymmetric and symmetric O—H groups stretching vibrations and the band at 2931.31 cm^{-1}, all of them were due to C—H—stretching of the AT and CCS chains. Important bands were observed at 1655.07 and at 1561.24 cm^{-1}, both due to asymmetric and symmetric C═O stretching of carbonyl group; two bands at 1436.81 and 1314.01 cm^{-1} which were attributed to O—H bending and C—O stretching of carboxylic acid and at 1224.18 cm^{-1} that was due to aromatic C—N stretching. This shift for the vibration peaks was attributed to the formation of hydrogen bonds between the AT and CCS chains (Fig. 1). In addition, the C═O stretching vibration peak showed a gradual change from 1667.71 to 1655.07 cm^{-1} (blue shift) indicating the possibility of interaction between AT-RM and CCS. Possibly, these results are related to ionic interactions between ionic superdisintegrants, such as SSG and CCS, and the surface of weak acidic drugs such as AT, previously observed in FTIR studies (Shaker et al., 2020; Zarmpi et al., 2020).

For the micellar solid dispersion MSD-AT:CCS:K (1:1:0.3), it was possible to observe an important shift at both 3388.13 and 2928.26 cm^{-1} bands, which were assigned to N—H vibrations (Kobayashi et al., 2017; da Silva et al., 2019) and a high C—H symmet-

ric stretching (Xu et al., 2019). Moreover, important changes were also observed for the intensity bands at 1655.13 and 1564.10 cm^{-1}, due to asymmetric and symmetric C═O stretching of carbonyl group. Previous studies showed how the increment of vibration for the aliphatic chain was related to an increase of surfactants on the surface of drug particles (Yang et al., 2019). Finally, there were observed bands at 1436.53 and 1314.85 cm^{-1} both of them due to O—H bending and C—O stretching. These slight displacement of C═O stretching from carbonyl group and C—N—H group, showed a gradual broadening, related to the SDS content (Fig. 1). The presence of Kolliphor® RH40 in MSD-AT:CCS:K (1:1:0.3) produced an important increase for the resulting bands at 2920.31, 1655.13, and 1060.95 cm^{-1} compared to SD-AT:CCS (1:1) formulation. This result indicated that the presence of the surfactant aliphatic C—H chains increased the intermolecular hydrogen bonding between AT and CCS chains. For MS-AT:CCS:K (1:1:0.3), the increase in the intensity of the absorption band for asymmetric and symmetric vibrations for carbonyl groups, compared to solid dispersion without surfactant, indicated that the surfactant is involved in an important raise of intermolecular hydrogen bonding between drug and polymer in AT solid dispersions (Sarabu et al., 2022; Yang et al., 2019). In addition, the improved wetting properties on the surface of the different solid dispersions, due to the presence of the surfactant, have been related to the presence of hydrogen bonds in the FTIR studies and would explain the improvement in the solubility results compared to SD-AT:CCS (1:1) (Sarabu et al., 2022).

Figs. 2 and 3 showed the XRPD and DSC diffractograms of the following samples: AT-RM, CCS, PM-AT:CCS:K 1:1:0.3, SD-AT:CCS (1:1) and MSD-AT:CCS:K (1:1:0.3). The AT-RM diffractogram exhibited two amorphous halos, between 6.5 and 13.0° 2θ and 15 – 25° 2θ, both characteristic of an amorphous structure. The absence of characteristic diffraction peaks confirms the presence of this amorphous form of AT. The DSC studies showed for the AT raw material, the absence of the endothermic peak at 156.9 °C, characteristic of a crystalline form of AT and only a broad endothermic event was observed at 217.6 °C, which could be attributed to the degradation product of AT (Faraji et al., 2021; Tizaoui et al., 2020).

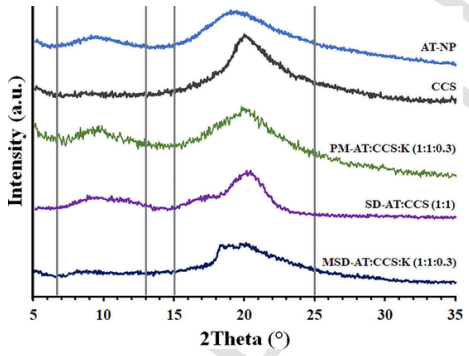

Fig. 2. XRPD diffraction patterns of Atorvastatin raw material (AT-RM); Croscarmellose (CCS); Physical mixture PM-AT:CCS:K (1:1:0.3); SD-AT:CCS (1:1); MSD-AT:CCS:K (1:1:0.1) and MSD-AT:CCS:K (1:1:0.3).

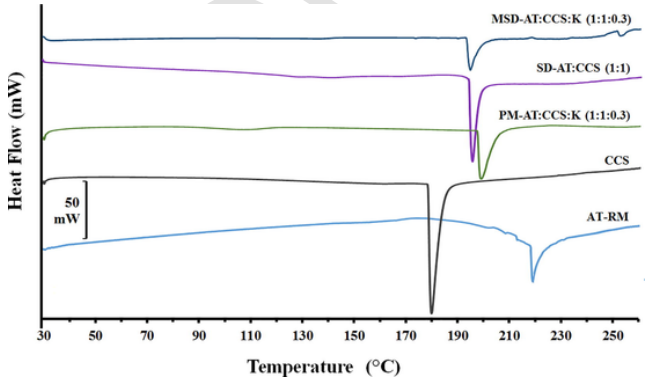

Fig. 3. DSC thermograms of Atorvastatin raw material (AT-RM); Croscarmellose (CCS); Physical mixture PM-AT:CCS:K (1:1:0.3); SD-AT:CCS (1:1); MSD-AT:CCS:K (1:1:0.1) and MSD-AT:CCS:K (1:1:0.3).

For hydrophilic CCS carrier, the XRPD data showed a broad halo between 15.0 and 25.0° 2θ (Sarabu et al., 2022) and a broad endothermic peak at 181.6 °C, both of them characteristic of a semicrystalline form, observed in different cellulosic polymers (Rashid et al., 2015).

The PM-AT:CCS:K (1:1:0.3) showed a slight decrease in the amorphous halo between 15.0 and 25.0° 2θ, which was attributed to an increase in the CCS chains motility, which enhances the interpenetration of AT molecules within the CCS chains (Ha et al., 2014; Yang et al., 2019). Similar amorphous halos were observed for both physical mixtures: PM-AT:CCS:K (1:1:0.1) and PM-AT:CCS:K (1:1:0.3). The surfactant effect on the CCS chain's mobility was confirmed in the DSC studies by an important displacement of the endothermic peak (197.9 °C), to intermediate values between CCS and AT-RM. This result was related to a high interaction between CCS and AT due to the presence of surfactant in PM-AT:CCS:K (1:1:0.3). The possible location of Kolliphor® RH40 on the surface of the PM-AT:CCS:K (1:1:0.3) could be due to the slight electrostatic attraction between the hydrophilic groups of the surfactant and the polar groups of the CCS polymer (Yang et al., 2019).

SD-AT:CCS (1:1) showed a slight decrease in the amorphous halo between 15.0 and 25.0° 2θ compared to PM-AT:CCS:K (1:1:0.3). In addition, the DSC study of SD-AT:CCS (1:1) also showed a slight endothermic peak shift at 195.6 °C. These results indicated that the elaboration of the solid dispersions increases the mobility of the CCS chains compared to PM-AT:CCS:K (1:1:0.3). Similar increases in the amorphous state of drugs have been previously observed in solid dispersion systems with low semicrystalline carrier ratios (Sarabu et al., 2022; Skotnicki et al., 2021).

The XRPD studies for MSD-AT:CCS:K (1:1:0.3) indicated that the presence of Kolliphor® RH40 surfactant was related to significant decreases in both amorphous halos between 6.5 and 13.0° and 16.0–25.0° 2θ. These decreases were related to an amorphous form of AT and a significant decrease in the semicrystalline character of CCS polymer chains. (Ha et al., 2014; Li et al., 2021). DSC results revealed a slight decrease in enthalpy values for the endothermic peak at 193.9 °C attributed to the high mobility of the CCS polymer chains due to the presence of the surfactant in these micellar systems (Rashid et al., 2015).

3.3. Dissolution studies

Dissolution profiles in biorelevant FaSSIF pH 6.5 medium of SD-AT:CCS (1:1) solid dispersion and both micellar solid dispersions MSD-AT:CCS:K (1:1:0.1) and MSD-AT:CCS:K (1:1:0.3), compared to AT-RM and PM-AT:CCS:K (1:1:0.3) physical mixture are observed in Fig. 4.

AT-RM showed an initial behaviour of slow dissolution releasing AT concentrations of 0.263 ± 0.006 mg/mL at 5 min. Afterwards, the solubility of AT exhibited concentrations of 0.409 ± 0.004 mg/mL at 2 h. Previous studies indicated that the presence of bile salts and lecithin micelles within FaSSIF biorelevant medium allowed to increase the solubility of certain lipophilic drugs by micellar solubilization (Lakshman et al., 2020).

PM-AT:CCS:K (1:1:0.3) showed increases in the initial dissolution profile with supersaturation concentrations of 0.428 ± 0.023 mg/mL at 10 min. After 10 min, aggregation and precipitation process were observed until 2 h with decreased concentration values (0.379 ± 0.011 mg/mL) (Elkhabaz et al., 2018; Skotnicki et al. 2021).

Solid dispersion SD-AT:CCS (1:1) exhibited a significant increase ($p < 0.05$) for concentration values at 15 min (0.542 ± 0.039 mg/mL). After the supersaturation peak, a decrease in AT concentration was observed, reaching values similar to PM-AT:CCS:K (1:1:0.3), which

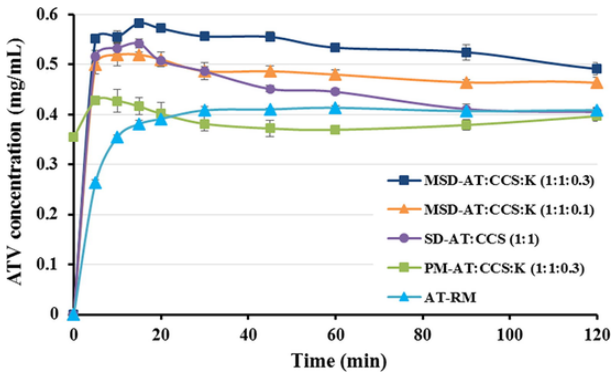

Fig. 4. Dissolution profiles of Atorvastatin raw material (AT-RM); Croscarmellose (CCS); Physical mixture PM-AT:CCS:K (1:1:0.3); SD-AT:CCS (1:1); MSD-AT:CCS:K (1:1:0.1) and MSD-AT:CCS:K (1:1:0.3).

indicates that a precipitation process occurred in this biorelevant medium (FaSSIF pH 6.5). The slow decrease in AT concentration could be related to a recrystallization of partially amorphous drug in the presence of crystal nucleus forming within the FaSSIF medium (Lakshman et al., 2020; Elkhabaz et al., 2018).

MSD-AT:CCS:K (1:1:0.1) micellar solid dispersion showed a fast dissolution profile with concentration values of 0.519 ± 0.006 mg/mL at 15 min. This low proportion of surfactant improves surface wettability and the formation of AT micelles. After the supersaturation peak, a rapid decrease was observed at 30 min, which was attributed to an aggregation of AT molecules. This recrystallization process was maintained until 2 h (0.463 ± 0.011 mg/mL). Possibly, the low proportion of surfactant in the solid dispersion moderated an earlier supersaturation depletion, which was related to a recrystallization of partially amorphous drug within the FaSSIF pH 6.5 medium. (Lakshman et al., 2020).

MSD-AT:CCS:K (1:1:0.3) micellar solid dispersion showed fast dissolution initial profiles with a high supersaturation concentration of 0.551 ± 0.006 mg/mL at 5 min. AT concentration in the dissolution medium achieved a relatively supersaturation concentration of 0.522 ± 0.006 mg/mL at 90 min and maintains the supersaturation conditions until 2 h (0.491 ± 0.012 mg/mL).The high proportion of surfactant in MSD-AT:CCS:K (1:1:0.3) could promote the presence of micelles that maintains AT supersaturating concentrations and therefore increases the maximum solubility advantage of amorphous AT for a longer time. Different studies indicate that the presence of surfactants produces a more delayed recrystallization and maintains concentrations above the AT solubility coefficient for a longer time (Rahman et al., 2020; Kwon et al., 2019; Aldosari et al., 2021).

3.4. Biochemical studies

In this study, rats were fed during eight weeks with a high-fat diet (HFD) composed of cholesterol and colic acid to induce hyperlipidaemia. After these eight weeks, animals were separated in three groups; one HFD group without treatment and two treatment groups: AT-RM and MSD-AT:CCS:K (1:1:0.3). These groups were compared with a Control group fed with a normal diet without cholesterol and colic acid addition.

Fig. 5 shows levels of TC, TG, LDL, HDL, AST and ALT for each group after eight weeks of atorvastatin treatment. At the end of the study, the TC level for HFD group showed a significant increase ($p < 0.05$) of 254.33 ± 19.09 mg/dL compared to Control group. The elevated TC, TG and LDL levels confirmed severe hypercholesterolemia after eight weeks of HFD feeding (Van den Hoek et al., 2021; Jahangiri et al., 2015; Zhou et al., 2014).

The AT-RM group, after eight weeks of treatment, did not present a significantly decrease ($p > 0.05$) for the TC values compared to HFD group. However, a significant decrease ($p < 0.05$) in TC (161.00 ± 12.39 mg/dL) was observed at the end of treatment with MSD-AT:CCS:K (1:1:0.3) compared to both HFD group and the group treated with AT-RM, respectively. The high TG value in the HFD group showed a significant increase ($p < 0.05$) of 166.25 ± 10.75 mg/dL compared to the level of the normal diet Control group. After eight weeks of treatment, the TG levels of both AT-RM and MSD-AT:CCS:K (1:1:0.3) groups showed significant reductions ($p < 0.05$) with 127.40 ± 15.18 and 88.00 ± 16.69 mg/dL levels, respectively, compared to HFD group (Fig. 5). The TG values of the MSD-AT:CCS:K (1:1:0.3) group also showed a significant decrease ($p < 0.05$) compared to the AT-RM group, showing similar TG levels to the Control group with a normal diet. The reduction of TC and TG values induces downregulation of lipogenesis genes to inhibit accumulation of hepatic lipid, decreasing TC and TG synthesis and allowing the microsomal TG transfer protein (MTTP) contribution to improve the lipid metabolism (Tzeng et al., 2015; Liu et al., 2018).

Previous studies have shown that long-term treatments improve the efficacy to obtain normal LDL and HDL levels (Zhou et al., 2014; Jahn et al., 2019). The LDL and HDL levels in the HFD group showed significant ($p < 0.05$) changes in comparison with the normal diet Control group, with increased LDL values (189.8 7 ± 19.23 mg/dL) and a decrease of 32.00 ± 2.65 mg/dL for HDL values, respectively (Fig. 5). At the end of the treatment, the AT-RM group presented non-significant ($p > 0.05$) differences in LDL and HDL levels compared to HFD group. However, the LDL levels in MSD-AT:CCS:K (1:1:0.3) group showed a significant decrease ($p < 0.05$) of 106.55 ± 13.21 mg/dL compared to the HFD group, also showing an important reduction of 37.19 % compared to AT-RM treatment group. In addition, after the treatment with MSD-AT:CCS:K (1:1:0.3), the HDL levels presented non-significant differences ($p > 0.05$) compared to the Control group. The addition of surfactant in MSD-AT:CCS:K (1:1:0.3) improves the membrane permeability transition of the active ingredient in rat hepatocytes. Furthermore, Kolliphor® RH40 could inhibit P-glycoprotein activity and increase the accumulation of substrate drugs such as AT (Torrado-Salmerón et al., 2019; Sayeed et al., 2017). These results indicated that this *in vivo* model of hyperlipidemia was especially suitable for evaluating the efficacy of AT treatment for micellar systems with different surfactants such as Poloxamer® 188, SDS and Kolliphor® RH40 (Torrado-Salmerón et al., 2019; Sharma et al., 2019; Salama et al., 2018).

Transaminase levels in the HFD group at the end of the study, showed a significant increase ($p < 0.05$) of 236.67 ± 15.36 mg/dL and 87.75 ± 5.68 mg/dL for AST and ALT values, respectively, compared to normal diet Control group (Fig. 5). After 8 weeks of treatment, the AT-RM group presented a significant decrease ($p < 0.05$) of AST levels (154.50 ± 17.62 mg/dL) but showed non-significant changes ($p > 0.05$) of ALT values in comparison with the HFD group. However, MSD-AT:CCS:K (1:1:0.3) treatment group presented significant decreases ($p < 0.05$) of AST (120.33 ± 9.50 mg/dL) and ALT (60.00 ± 7.07 mg/dL) values compared to the HFD group, showing AST and ALT levels similar to the Control group. These decreases for ALT values were related to a high fat clearance within hepatocytes (Mohamed et al., 2019; Klaebel et al., 2019).

3.5. Histopathological studies

At the end of the *in vivo* studies, liver tissue sections, stained with haematoxylin-eosin, were examined histologically (Fig. 6).

The histopathological study of the normal diet Control group exhibited regular liver tissue without steatosis, lobular inflammation or ballooning, these tissue sections were categorized as NAS = 0. However, the HFD group showed fat adipocytes and microvesicular steatosis, but also microgranulomas with lipid droplets and ballooned hepatocytes.

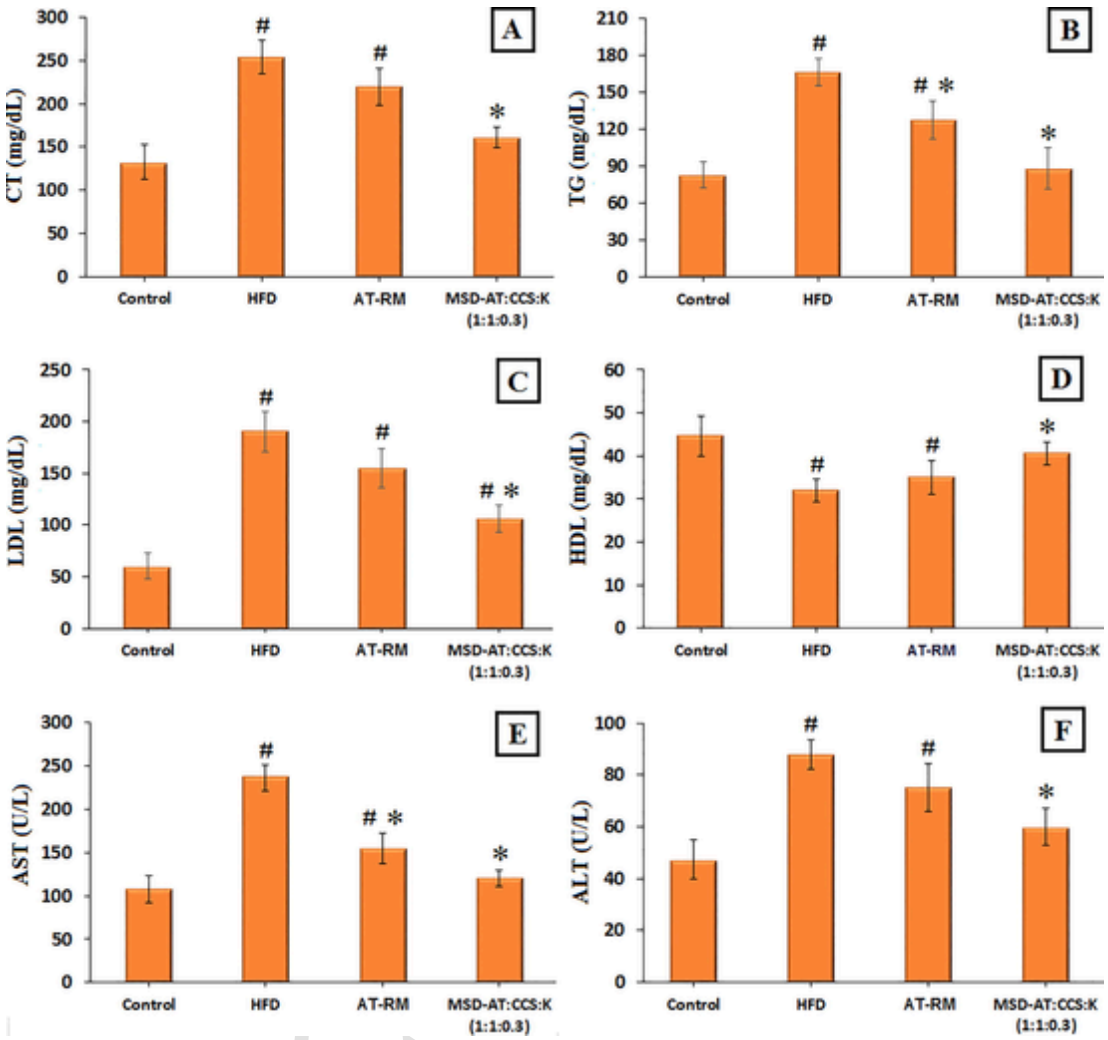

Fig. 5. Serum levels of (A) Total Cholesterol (TC); (B) Triglyceride (TG); (C) Low-Density Lipoprotein (LDL); (D) High-Density Lipoprotein (HDL), (E) Aspartate transaminase (AST) and (F) Alanine transaminase (ALT) after 4 weeks of treatment. Mean and standard error (n = 6) of the following Wistar rats groups: Control group; High fat diet (HFD) group; AT raw material (AT-RM) group and Micellar Solid dispersion (MSD-AT:CCS:K (1:1:0.3)) group. ANOVA was used for multiple comparison. (#) significant ($p < 0.05$) compared with Control group; (*) significant ($p < 0.05$) compared with HFD group.

The histological results of this HFD group have been categorized as NAS = 7 (Fig. 6). These findings are consistent with the high levels of TC and lipids observed in biochemical studies and the increase in AST and ALT values, therefore all of them are related to the liver damage. (Klaebel et al., 2019; Tzeng et al., 2015).

The AT-RM group showed a decrease in liver damage compared to HFD, but despite everything, this treatment group maintains a high steatosis level. The AT-RM group showed a similar microvesicular steatosis with small lipid droplets inside the hepatocytes, but less clusters of inflammatory cells and ballooning injury were observed on liver histopathological examination compared to normal diet Control group. As a result, the histopathological study of AT-RM presented a high NAS level of 5.5. Similar decreases in inflammation and ballooning injury scores were observed in previous studies with AT treatments (Mohamed et al., 2019; Klaebel et al., 2019).

On the other hand, the histology studies of liver tissue in MSD-AT:CCS:K (1:1:0.3) group presented an important reduction of the liver damage compared to HFD and AT-RM groups. The MSD-AT:CCS:K (1:1:0.3) group showed a moderate level of microvesicular steatosis and a decrease in inflammatory cell infiltration. However, this treatment group presented similar levels of hepatocellular ballooning in comparison with AT-RM group (Fig. 6). These results of liver damage presented a NAS value of 4. This score is under the threshold value of ≥ 5 in the diagnosis of NASH. The significant decrease ($p < 0.05$) in the NAS score of MSD-AT:CCS:K (1:1:0.3) group compared to AT-RM group, indicated that treatment with AT micellar systems could reduce lipid and transaminase levels and achieve a diminished steatosis levels (Torrado-Salmerón et al., 2021; Klaebel et al., 2019). Previous studies indicate that the significant decrease in AST and ALT values, have been related to a significant improvement in NASH diseases (Tzeng et al., 2015; Jahn et al., 2019).

4. Conclusions

In this study, the addition of Kolliphor® RH40, as a potent surfactant, to AT:CCS solid dispersions was successfully developed, improving the AT dissolution profile and increasing its efficacy. Solubility and wettability studies showed that the CCS cellulose polymer is a highly hydrophilic carrier which allows the development of solid dispersions with low drug/carrier ratios. FTIR studies indicated that the Kolliphor® RH40 presence in MSD-AT:CCS:K (1:1:0.3) produced important increases on vibration for either the aliphatic chain, amidogen, hydroxyl and carbonyl groups. These results indicated that surfactant is involved in an important raise of intermolecular hydrogen bonding between drug and polymer chains. Both DSC and FTIR data have shown that the Kolliphor® RH40 surfactant addition enhanced CCS chains mobility,

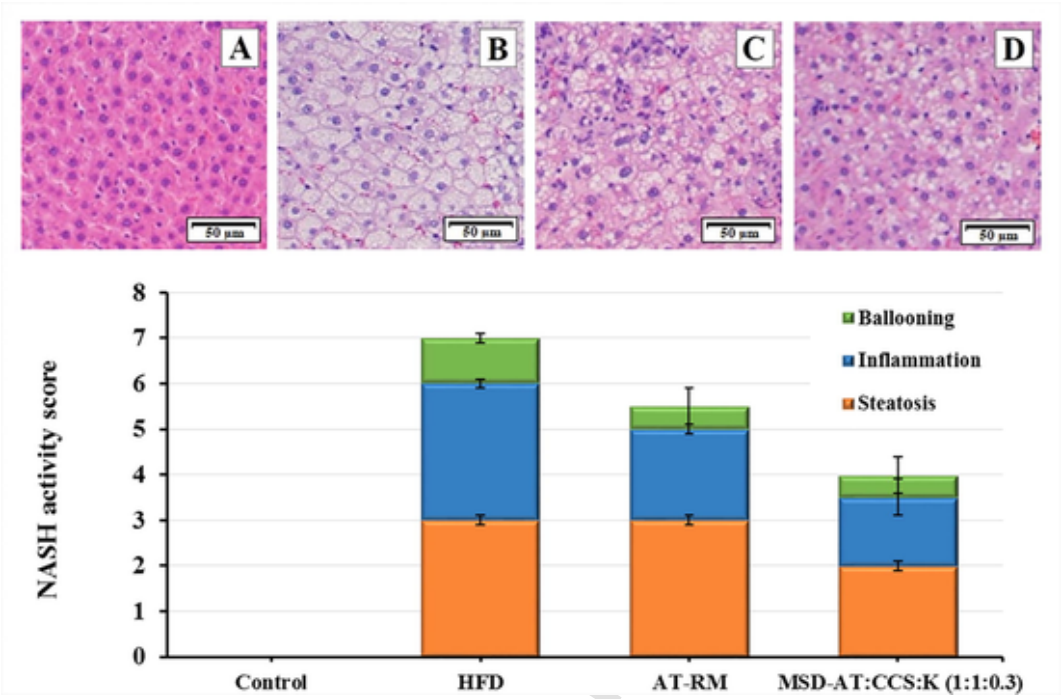

Fig. 6. Histological representation (hematoxylin and eosin 20 ×) of liver tissues in Wistar rats after 4 weeks of treatment. (A) Control group; (B) High fat diet (HFD) group; (C) AT raw material (AT-RM) group and (D) Micellar Solid dispersion (MSD-AT:CCS:K (1:1:0.3)) group. Histological evaluation of the liver sections. Results are expressed as the mean of NASH score ± SD (n = 6).

thus, increasing the AT molecules movement into the CCS polymer structure, producing considerable decreases in crystallinity.

The dissolution in biorelevant FaSSIF medium pointed out that Kolliphor® RH40 surfactant presence in MSD-AT:CCS:K (1:1:0.1) produced unstable micelle systems that increased the supersaturation peak during the first stage of dissolution studies, followed by a precipitation process. However, only MSD-AT:CCS:K (1:1:0.3) achieved a delayed recrystallization, maintaining supersaturation concentrations which is largely controlled either by drug-polymer interactions/micellar structures solubility for a longer time.

Efficacy studies showed that MSD-AT:CCS:K (1:1:0.3) micellar system produced a significant ($p < 0.05$) decrease in serum levels of either total cholesterol (TC), low-density lipoproteins (LDLs), and triglycerides (TGs) compared to AT-RM groups. At the end of this treatment, these micellar systems reached levels of total cholesterol (TC) and triglycerides (TG) similar to the control group. However, these micellar systems exhibited slightly higher levels of low-density lipoproteins (LDL) than the control group. Micellar systems treatment achieved a high improvement in the lipid profile compared to the AT-RM treatment group, which could be attributed to micellar structures which increased AT supersaturation peaks and improved their efficacy. The histopathological study showed an important NAS score for the HFD group. The AT-RM treatment group showed a significant decrease in inflammation and ballooning damage compared to HFD group. However, the Kolliphor® RH40 surfactant presence in MSD-AT:CCS:K (1:1:0.3) resulted in a significant ($p < 0.05$) decrease in hepatic steatosis and inflammatory injury compared to AT-RM group. These studies suggested that micellar systems using Kolliphor® RH40 could enhance the AT antihyperlipidemic efficacy and decrease nonalcoholic steatosis.

Funding

This work was supported by the Spanish Ministries of Science and Innovation: MICINU, [RTI2018-093940-B-100]; and the University Complutense of Madrid [Research Group 910939]. Carlos Torrado-Salmerón acknowledges a grant awarded by the Rafael Folch Foundation.

Institutional Review Board Statement

The animal study was conducted in the Animal Experimentation Centre at the University of Alcalá de Henares according to the guidelines of the Ethical Committee (Directive 2010/63/EU), with the project identification of Community of Madrid PROEX 041/18 project identification code ES280050001165 (27 April 2018).

CRediT authorship contribution statement

Carlos Torrado-Salmerón : Conceptualization, Methodology, Investigation, Writing – original draft, Writing – review & editing, Visualization. **Víctor Guarnizo-Herrero :** Methodology, Investigation, Writing – original draft, Visualization. **Guillermo Torrado :** Conceptualization, Methodology, Resources, Supervision, Funding acquisition. **Ma Ángeles Peña :** Conceptualization, Methodology, Investigation, Writing – original draft. **Santiago Torrado-Santiago :** Conceptualization, Writing – original draft, Writing – review & editing, Supervision, Funding acquisition. **Paloma Ma Torre Iglesias :** Conceptualization, Investigation, Writing – original draft, Writing – review & editing, Visualization, Supervision.

Declaration of Competing Interest

The authors declare that they have no known competing financial interests or personal relationships that could have appeared to influence the work reported in this paper.

Data availability

Data will be made available on request.

Acknowledgments

The authors thank Normon Pharmaceutical Co., Ltd. for providing the materials free of charge.

Appendix A. Supplementary material

Supplementary data to this article can be found online at https://doi.org/10.1016/j.ijpharm.2022.122520.

Reference

Agrawal, A.M., Dudhedia, M.S., Zimny, E., 2016. Hot melt extrusion: development of an amorphous solid dispersion for an insoluble drug from mini-scale to clinical scale. AAPS PharmSciTech. 17 (1), 133–147. https://doi.org/10.1208/s12249-015-0425-7.

Aldosari, B.N., Almurshedi, A.S., Alfagih, I.M., AlQuadeib, B.T., Altamimi, M.A., Imam, S.S., Hussain, A., Alqahtani, F., Alzait, E., Alshehri, S., 2021. Formulation of Gelucire®-based solid dispersions of atorvastatin calcium: in vitro dissolution and in vivo bioavailability study. AAPS PharmSciTech. 22 (5), 1–13. https://doi.org/10.1208/s12249-021-02019-5.

Blasco, A., Torrado, G., Peña Ma, A., 2020. Formulation and Evaluation of Loperamide HCl Oro Dispersible Tablets. Pharmaceuticals. 13 (5), 100. https://doi.org/10.3390/ph13050100.

Chaturvedi, M., Kumar, M., Pathak, K., Bhatt, S., Saini, V., 2017. Surface solid dispersion and solid dispersion of meloxicam: comparison and product development. Adv. Pharm. Bull. 7 (4), 569. https://doi.org/10.15171/apb.2017.068.

da Silva, K. M. A.; de Lima Ramos Júnior, F. J.; Chavez Júnior J. V.; Brandão, D. O.; Lins, T. B.; Macêdo, R. O.; de Souza, F. S. Characterization of solid dispersions of a powerful statin using thermoanalytical techniques. J. Therm. Anal. Calorim. 2019, 138 (5), 3701–3714. Doi: 10.1007/s10973-019-08450-y.

Dong, W., Su, X., Xu, M., Hu, M., Sun, Y., Zhang, P., 2018. Preparation, characterization, and in vitro/vivo evaluation of polymer-assisting formulation of atorvastatin calcium based on solid dispersion technique. Asian J. Pharm. Sci. 13 (6), 546–554. https://doi.org/10.1016/j.ajps.2018.08.010.

Doumas, M., Imprialos, K., Dimakopoulou, A., Stavropoulos, K., Binas, A., Athyros, V.G., 2018. The role of statins in the management of nonalcoholic fatty liver disease. Curr. Pharm. Design. 24 (38), 4587–4592. https://doi.org/10.2174/1381612825666190117114305.

Elkhabaz, A., Sarkar, S., Dinh, J.K., Simpson, G.J., Taylor, L.S., 2018. Variation in supersaturation and phase behavior of ezetimibe amorphous solid dispersions upon dissolution in different biorelevant media. Mol. Pharmaceut. 15 (1), 193–206. https://doi.org/10.1021/acs.molpharmaceut.7b00814.

Elmowafy, M., Ibrahim, H.M., Ahmed, M.A., Shalaby, K., Salama, A., Hefesha, H., 2017. Atorvastatin-loaded nanostructured lipid carriers (NLCs): strategy to overcome oral delivery drawbacks. Drug Deliv. 24 (1), 932–941. https://doi.org/10.1080/10717544.2017.1337823.

Faraji, E., Mohammadi, M., Mahboobian, M.M., 2021. Development of the Binary and Ternary Atorvastatin Solid Dispersions. In Vitro and In Vivo Investigations. Biomed Res. Int. 6644630. https://doi.org/10.1155/2021/6644630.

França MT, Nicolay Pereira R, Klüppel Riekes M, Munari Oliveira Pinto J, Stulzer HK. Investigation of novel supersaturating drug delivery systems of chlorthalidone: The use of polymer-surfactant complex as an effective carrier in solid dispersions. Eur J Pharm Sci. 2018 Jan 1;111:142-152. doi: 10.1016/j.ejps.2017.09.043. Epub 2017 Sep 28. PMID: 28964949.

Ha, E.S., Baek, I.H., Cho, W., Hwang, S.J., Kim, M.S., 2014. Preparation and evaluation of solid dispersion of atorvastatin calcium with Soluplus® by spray drying technique. Chem. Pharm. Bull. 62 (6), 545–551. https://doi.org/10.1248/cpb.c14-00030.

Han, T., Yong, J., Liu, Q., Gu, X., Zhang, W., Yang, J., 2020. Preparation and characterization of wet-milled cyclovirobuxine D nanosuspensions. J. Therm. Anal. Calorim. 139 (3), 1959–1970. https://doi.org/10.1007/s10973-019-08574-1.

Ikeuchi, S.Y., Kambayashi, A., Kojima, H., Oku, N., Asai, T., 2018. Prediction of the oral pharmacokinetics and food effects of gabapentin enacarbil extended-release tablets using biorelevant dissolution tests. Biol. Pharm. Bull. 41 (11), 1708–1715. https://doi.org/10.1248/bpb.b18-00456.

Indulkar, A.S., Lou, X., Zhang, G.G., Taylor, L.S., 2022. Role of Surfactants on Release Performance of Amorphous Solid Dispersions of Ritonavir and Copovidone. Pharm. Res. 39 (2), 381–397. https://doi.org/10.1007/s11095-022-03183-4.

Iqbal, A., Hossain, S., Shamim, A., Islam, M., Siddique, A.T., 2020. Formulation, in vitro evaluation and characterization of atorvastatin solid dispersion. Trop. J. Pharm. Res. 19 (6), 1131–1138. https://doi.org/10.4314/tjpr.v19i6.2.

Jahangiri, A., Barzegar-Jalali, M., Garjani, A., Javadzadeh, Y., Hamishehkar, H., Afroozian, A., Adibkia, K., 2015. Pharmacological and histological examination of atorvastatin-PVP K30 solid dispersions. Powder Technol. 286, 538–545. https://doi.org/10.1016/j.powtec.2015.08.047.

Jahn, D., Dorbath, D., Kircher, S., Nier, A., Bergheim, I., Lenaerts, K., Hermanns, H.M., Geier, A., 2019. Beneficial effects of vitamin D treatment in an obese mouse model of non-alcoholic steatohepatitis. Nutrients. 11 (1), 77. https://doi.org/10.3390/nu11010077.

Kim, M.S., Kim, J.S., Cho, W., Park, H.J., Hwang, S.J., 2013. Oral absorption of atorvastatin solid dispersion based on cellulose or pyrrolidone derivative polymers. Int. J. Biol. Macromol. 59, 138–142. https://doi.org/10.1016/j.ijbiomac.2013.03.068.

Klaebel, J.H., Skjødt, M., Skat-Rørdam, J., Rakipovski, G., Ipsen, D.H., Schou-Pedersen, A.M.V., Lykkesfeldt, J., Tveden-Nyborg, P., 2019. Atorvastatin and vitamin E accelerates NASH resolution by dietary intervention in a preclinical guinea pig model. Nutrients. 11 (11), 2834. https://doi.org/10.3390/nu11112834.

Kobayashi, M., Hattori, Y., Sasaki, T., Otsuka, M., 2017. Effect of ball milling on the physicochemical properties of atorvastatin calcium sesquihydrate: the dissolution kinetic behaviours of milled amorphous solids. J. Pharm. Pharmacol. 69 (1), 15–22. https://doi.org/10.1111/jphp.12636.

Krollik, K., Lehmann, A., Wagner, C., Kaidas, J., Kubas, H., Weitschies, W., 2022. The effect of buffer species on biorelevant dissolution and precipitation assays–Comparison of phosphate and bicarbonate buffer. Eur. J. Pharm. Biopharm. 171, 90–101. https://doi.org/10.1016/j.ejpb.2021.09.009.

Kumar, N., Chaurasia, S., Patel, R.R., Khan, G., Kumar, V., Mishra, B., 2017. Atorvastatin calcium encapsulated eudragit nanoparticles with enhanced oral bioavailability, safety and efficacy profile. Pharm. Dev. Technol. 22 (2), 156–167. https://doi.org/10.3109/10837450.2015.1108983.

Kurakula, M., El-Helw, A.M., Sobahi, T.R., Abdelaal, M.Y., 2015. Chitosan based atorvastatin nanocrystals: effect of cationic charge on particle size, formulation stability, and in-vivo efficacy. Int. J. Nanomed. 10, 321–334. https://doi.org/10.2147/IJN.S77731.

Kwon, J., Giri, B.R., Song, E.S., Bae, J., Lee, J., Kim, D.W., 2019. Spray-dried amorphous solid dispersions of atorvastatin calcium for improved supersaturation and oral bioavailability. Pharmaceutics. 11 (9), 461. https://doi.org/10.3390/pharmaceutics11090461.

Lakshman, D., Chegireddy, M., Hanegave, G.K., Sree, K.N., Kumar, N., Lewis, S.A., Dengale, S.J., 2020. Investigation of drug-polymer miscibility, biorelevant dissolution, and bioavailability improvement of Dolutegravir-polyvinyl caprolactam-polyvinyl acetate-polyethylene glycol graft copolymer solid dispersions. Eur. J. Pharm. Sci. 142, 105137. https://doi.org/10.1016/j.ejps.2019.105137.

Li, W., Song, J., Li, J., Li, M., Tian, B., He, Z., Liu, X., Fu, Q., 2021. Co-amorphization of atorvastatin by lisinopril as a co-former for solubility improvement. Int. J. Pharmaceut. 607, 120971. https://doi.org/10.1016/j.ijpharm.2021.120971.

Liu, S.H., Chiu, C.Y., Shi, C.M., Chiang, M.T., 2018. Functional comparison of high and low molecular weight chitosan on lipid metabolism and signals in high-fat diet-fed rats. Marine Drugs. 16 (8), 251. https://doi.org/10.3390/md16080251.

Ma, Y., Yang, Y., Xie, J., Xu, J., Yue, P., Yang, M., 2018. Novel nanocrystal-based solid dispersion with high drug loading, enhanced dissolution, and bioavailability of andrographolide. Int. J. Nanomed. 13, 3763–3779. https://doi.org/10.2147/IJN.S164228.

Mohamed, A.S., Ibrahim, W.M., Zaki, N.I., Ali, S.B., Soliman, A.M., 2019. Effectiveness of coelatura aegyptiaca extract combination with atorvastatin on experimentally induced hyperlipidemia in rats. Evid Based Complement Alternat Med. 9726137. https://doi.org/10.1155/2019/9726137.

Pas, T., Verbert, S., Appeltans, B., Van den Mooter, G., 2020. The influence of crushing amorphous solid dispersion dosage forms on the in-vitro dissolution kinetics. Int J Pharmaceut. 573, 118884. https://doi.org/10.1016/j.ijpharm.2019.118884.

Rahman, M., Coelho, A., Tarabokija, J., Ahmad, S., Radgman, K., Bilgili, E., 2020. Synergistic and antagonistic effects of various amphiphilic polymer combinations in enhancing griseofulvin release from ternary amorphous solid dispersions. Eur. J. Pharm. Sci. 150, 105354. https://doi.org/10.1016/j.ejps.2020.105354.

Rashid, R.; Kim, D. W.; ud Din, F.; Mustapha, O.; Yousaf, A. M.; Park, J. H.; Kim J. O.; Yong C. S.; Choi, H. G. Effect of hydroxypropylcellulose and Tween 80 on physicochemical properties and bioavailability of ezetimibe-loaded solid dispersion. Carbohyd. Polym. 2015, 130, 26–31. Doi: 10.1016/j.carbpol.2015.04.071.

Salama, A.H., Basha, M., El Awdan, S., 2018. Experimentally designed lyophilized dry emulsion tablets for enhancing the antihyperlipidemic activity of atorvastatin calcium: Preparation, in-vitro evaluation and in-vivo assessment. Eur. J. Pharm. Sci. 112, 52–62. https://doi.org/10.1016/j.ejps.2017.11.003.

Sarabu, S., Butreddy, A., Bandari, S., Batra, A., Lawal, K., Chen, N.N., Kogan, M., Bi, V., Repka, M.A., 2022. Preliminary investigation of peroxide levels of Plasdone™ copovidones on the purity of atorvastatin calcium amorphous solid dispersions: Impact of plasticizers on hot melt extrusion processability. J. Drug Deliv. Sci. Technol. 70, 103190. https://doi.org/10.1016/j.jddst.2022.103190.

Sayeed, S., Imam, S.S., Najmi, A.K., Aqil, M., Akhtar, M., 2017. Nonionic surfactant based thymoquinone loaded nanoproniosomal formulation: in vitro physicochemical evaluation and in vivo hepatoprotective efficacy. Drug Dev. Ind. Pharm. 43 (9), 1413–1420. https://doi.org/10.1080/03639045.2017.1318903.

Shaker, M.A., Elbadawy, H.M., Shaker, M.A., 2020. Improved solubility, dissolution, and oral bioavailability for atorvastatin-Pluronic® solid dispersions. Int. J. Pharmaceut. 574, 118891. https://doi.org/10.1016/j.ijpharm.2019.118891.

Sharma, M., Mehta, I., 2019. Surface stabilized atorvastatin nanocrystals with improved bioavailability, safety and antihyperlipidemic potential. Sci. Rep. 9 (1), 16105. https://doi.org/10.1038/s41598-019-52645-0.

Skotnicki, M., Jadach, B., Skotnicka, A., Milanowski, B., Tajber, L., Pyda, M., Kujawski, J., 2021. Physicochemical characterization of a co-amorphous atorvastatin-irbesartan system with a potential application in fixed-dose combination therapy. Pharmaceutics. 13 (1), 118. https://doi.org/10.3390/pharmaceutics13010118.

Srivalli, K.M., Mishra, B., 2015. Preparation and pharmacodynamic assessment of ezetimibe nanocrystals: effect of P-gp inhibitory stabilizer on particle size and oral absorption. Colloids Surf. B Biointerfaces. 135, 756–764. https://doi.org/10.1016/j.colsurfb.2015.08.042.

Tizaoui, C., Galai, H., Barrio, M., Clevers, S., Couvrat, N., Dupray, V., Tamarit, J.L., Rietveld, I.B., 2020. Does the trihydrate of atorvastatin calcium possess a melting point? Eur. J. Pharm. Sci. 148, 105334. https://doi.org/10.1016/j.ejps.2020.105334.

Torrado-Salmerón, C., Guarnizo-Herrero, V., Cerezo-Garreta, J., Torrado Durán, G., Torrado-Santiago, S., 2019. Self-micellizing technology improves the properties of

ezetimibe and increases its effect on hyperlipidemic rats. Pharmaceutics. 11 (12), 647. https://doi.org/10.3390/pharmaceutics11120647.
Torrado-Salmerón, C., Guarnizo-Herrero, V., Henriques, J., Seiça, R., Sena, C.M., Torrado-Santiago, S., 2021. Multiparticulate Systems of Ezetimibe Micellar System and Atorvastatin Solid Dispersion Efficacy of Low-Dose Ezetimibe/Atorvastatin on High-Fat Diet-Induced Hyperlipidemia and Hepatic Steatosis in Diabetic Rats. Pharmaceutics. 13 (3), 421. https://doi.org/10.3390/pharmaceutics13030421.
Tzeng, T.F., Liou, S.S., Chang, C.J., Liu, I.M., 2015. 6-gingerol protects against nutritional steatohepatitis by regulating key genes related to inflammation and lipid metabolism. Nutrients. 7 (2), 999–1020. https://doi.org/10.3390/nu7020999.
Van den Hoek, A.M., Verschuren, L., Caspers, M.P., Worms, N., Menke, A.L., Princen, H.M., 2021. Beneficial effects of elafibranor on NASH in E3L. CETP mice and differences between mice and men. Sci. Rep. 11 (1), 1–14. https://doi.org/10.1038/s41598-021-83974-8.
Xu, C., Wang, D., Wang, H., Ma, L., Zhu, X., Zhu, Y., Zhang, Y., Liu, F., 2019. Experimental investigation of coal dust wetting ability of anionic surfactants with different structures. Process. Saf. Environ. 121, 69–76. https://doi.org/10.1016/j.psep.2018.10.010.
Yang, B., Wei, C., Qian, F., Li, S., 2019. Surface wettability modulated by surfactant and its effects on the drug release and absorption of fenofibrate solid dispersions. AAPS PharmSciTech. 20 (6), 234. https://doi.org/10.1208/s12249-019-1446-4.
Yin, Y., Liu, H., Zheng, Z., Lu, R., Jiang, Z., 2019. Genistein can ameliorate hepatic inflammatory reaction in nonalcoholic steatohepatitis rats. Biomed. Pharmacother. 111, 1290–1296. https://doi.org/10.1016/j.biopha.2019.01.004.
Zarmpi, P., Flanagan, T., Meehan, E., Mann, J., Fotaki, N., 2020. Biopharmaceutical understanding of excipient variability on drug apparent solubility based on drug physicochemical properties Case study: superdisintegrants. AAPS J. 22 (2), 46. https://doi.org/10.1208/s12248-019-0406-y.
Zhou, S., Zhao, P., Li, Y., Deng, T., Tian, L., Li, H., 2014. Renoprotective effect of atorvastatin on STZ-diabetic rats through attenuating kidney-associated dysmetabolism. Eur. J. Pharmacol. 740, 9–14. https://doi.org/10.1016/j.ejphar.2014.06.055.